Long non-coding RNA PTTG3P promotes hepatocellular carcinoma growth via modulating nuclear-cytoplasm shuttle of ILF2 and stabilizing TOP2A mRNA

hansong bai (49063656@qq.com)
Sichuan Cancer Hospital and Research Institute: Sichuan Cancer Hospital and Institute
https://orcid.org/0000-0002-3965-738X

hangyue zhang
Southwest Medical University School of Clinical Medical Sciences

jiahua Lyu
Sichuan Cancer Hospital and Research Institute: Sichuan Cancer Hospital and Institute

Long Liang
Sichuan Cancer Hospital and Research Institute: Sichuan Cancer Hospital and Institute

Hongyuan Jia
Sichuan Cancer Hospital and Research Institute: Sichuan Cancer Hospital and Institute

Ming Zeng
Sichuan Provincial People's Hospital: Sichuan Academy of Medical Sciences and Sichuan People's Hospital

Tao Li
Sichuan Cancer Hospital and Research Institute: Sichuan Cancer Hospital and Institute

Research Article

Keywords: PTTG3P, ILF2, ILF3, TOP2A, hepatocellular carcinoma

Posted Date: May 3rd, 2022

DOI: https://doi.org/10.21203/rs.3.rs-1542711/v1

Abstract

Background*: PTTG3P* has been characterized as an oncogenic lncRNA in hepatocellular carcinoma (HCC). However, the underlying mechanisms have not been fully understood. This study aimed to explore the functional partner of *PTTG3P* in modulating HCC malignant phenotypes.

Methods: Hep3B and HepG2 were used as representative HCC models. Cellular and molecular studies were performed using RNA pull-down/mass spectrometry (MS), RNA immunoprecipitation (RIP)-qPCR, Chromatin immunoprecipitation (ChIP)-qPCR, and immunofluorescent (IF) staining.

Results: *PTTG3P* interacts with both ILF2 and ILF3. The binding between *PTTG3P* and ILF2 helps maintain the cytoplasmic distribution of ILF2. Together with ILF2, *PTTG3P* binds to the 3'UTR of TOP2A. *PTTG3P* depletion impairs the binding and reduces *TOP2A* mRNA stability. Meanwhile, *PTTG3P* depletion is associated with nuclear accumulation of ILF2 and increased binding of ILF2 to the promoter region of *TOP2A*. Dual-luciferase assay confirmed that ILF2 activates the *TOP2A* promoter and increases its transcription.

Conclusion: this study revealed that when *PTTG3P* is overexpressed in HCC tumor cells, it mainly acts as a *TOP2A* mRNA stabilizer, via recruiting the ILF2/ILF3 complex to the 3'UTR of *TOP2A* mRNA. However, *PTTG3P* depletion results in nuclear accumulation of ILF2 and subsequent transcriptional activation of *TOP2A*. This might be utilized by HCC cells to compensate the loss of *PTTG3P* and associated *TOP2A* instability. These findings help expand our understanding of the oncogenic mechanisms of *PTTG3P* in HCC.

Introduction

Long non-coding RNAs (lncRNAs) are transcripts with more than 200 nucleotides that are not translated into proteins. During the past decades, a large number of studies have revealed that lncRNAs exert critical regulatory mechanisms in various cellular activities or diseases [1]. Many lncRNAs are aberrantly expressed in hepatocellular carcinoma (HCC) and regulate the carcinogenic and pathological processes [2,3]. The regulatory mechanisms of lncRNAs are complex and can be at both genetic and epigenetic levels. Firstly, they bind to DNA and remodel chromatin, leading to altered gene expression [4,5]. Secondly, some lncRNAs may encode functional peptides[6]. Thirdly, they can bind to mRNAs and influence their stability and transcription [7,8]. Fourthly, they sponge miRNAs and regulate their stability and targeting [9]. Fifthly, they interact with proteins, modulating their conformation, localization, or stability [10,11].

Our previous study found that lncRNA *PTTG3P* upregulation is a biomarker of unfavorable prognosis of HCC [12]. It stimulates PTTG1 expression and activates PI3K/AKT signaling [13] and sponges miR-383 and upregulates *CCND1* and *PARP2* expression in HCC [14]. *PTTG3P* also interacts with FOXM1 and activates the transcription of the mitotic checkpoint kinase gene *BUB1B*, leading to facilitated tumor growth and enhanced chemoresistance in lung adenocarcinoma (LUAD) [15].

Interleukin Enhancer Binding Factor 2 (ILF2, also known as NF45) can form a complex with ILF3 (NF90). ILF2/ILF3 complex acts as a transcriptional activator via binding to the antigen receptor response element (ARRE)-2 (5'-AAGAAAGGAGGAAAAACTGTTT-3') of the proximal promoter of multiple genes, including IL2 [16], IL13 [17] and *FOS* [18]. This complex recognizes and binds to the core sequences, including CTGTT and GGAAA motif [17,19]. The tumor-promoting effect of ILF2 and ILF3 has been reported in HCC [20]. This complex induces the elevation of EGF receptor levels and promotes cell proliferation via binding to pri-miR-7-1 and suppressing mature miR-7-1 generation [20,21]. ILF2/ILF3 binds to the 3' untranslated regions (3'UTRs) of multiple mRNAs and increases their stability, leading to facilitated cell-cycle progression and cell proliferation [21].

Here, we confirmed that *PTTG3P* contributes to the malignant phenotype of HCC, typically via enhancing cell proliferation and invasion. Mechanistically, *PTTG3P* interacts with ILF2 and ILF3, which bind to the 3'UTR of *TOP2A* (encoding DNA Topoisomerase II α) mRNA and increase its stability. *PTTG3P* depletion triggers nuclear translocation of ILF2, which binds to the promoter of the *TOP2A* gene and enhances its transcription.

Materials And Methods

Bioinformatic analysis

Data extraction from TCGA-LIHC and survival analysis followed the methods as described previously [12].

Cell culture and treatment

Human HCC cell lines, Hep3B and HepG2 were obtained from ATCC (Manassas, VA, USA) and grown in Dulbecco's modified Eagle's medium (DMEM, Corning, Manassas, VA, USA) with 10% FBS. All cell lines were maintained at 37°C and 5% CO_2 in an incubator.

Lentiviral *PTTG3P* (NR_002734.2) overexpression plasmid was generated using the shuttle plasmid pLVX-Puro. Lentiviral *PTTG3P*, *ILF2,* and *TOP2A* were constructed using pLKO.1-puro plasmid. The validated shRNA sequences were provided in Table S1. Empty vectors and scramble (scr.) sequences were used as controls, respectively.

Lentiviruses were produced by co-transfecting recombinant shuttle plasmids with lentivirus packaging plasmids (pSPAX2 and pMD2G, HanBio Technology) in 293T cells. Briefly, supernatants 48 h after transfection were harvested, centrifuged, filtered through a 0.45 μm filter and finally ultracentrifuged. Then the lentiviral plasmids were dissolved in PBS and stored at -80 °C. Hep3B and HepG2 cells were infected with lentiviruses at a multiplicity of infection (MOI) of 15.

RNA fluorescence in situ hybridization (RNA-FISH)

RNA-FISH assay was performed according to the methods described previously [22]. CY3-conjugated *PTTG3P* probes were generated according to protocols from RiboBio (Guangzhou, China). The following probe sequence was used: 5'- -3'. Nuclei were stained with 6-diamidino-2-phenylindole (DAPI). Fluorescent images were captured using a fluorescence microscope (Olympus IX83, Tokyo, Japan).

RNA extraction and quantitative Real-Time PCR (qRT-PCR)

In brief, Total RNA was extracted by using the RNeasy minikit (QIAGEN, Hilden, Germany) and was reverse transcribed into the first strand DNA by using a cDNA reverse transcription kit (Applied Biosystems, Foster City, CA, USA) following the manufacturer's instructions. qRT-PCR was performed with TaqMan gene expression master mix (Applied Biosystems), on an ABI Real-Time 7900HT cycler. RNA levels of queried genes were normalized to the level of *GAPDH*. Results are representative of three individual experiments in triplicate. The primers used in this study were provided in Supplementary Table 1.

CCK-8 assay of cell proliferation

Cell Counting Kit-8 (CCK-8; Beyotime Institute of Biotechnology) was used to measure cell proliferation following the manufacturer's instructions. Briefly, 24 h after lentiviral infection, cells were plated in 96-well plates (2×10^3 cells/well) in a medium containing 10% FBS for 24, 48 or 72 h. Then 10 μL CCK-8 solution was added to each well and incubated for 2 h. The absorbance at 450 nm was measured using a microplate reader. Results are representative of three individual experiments in triplicate.

Flow-cytometric analysis of cell-cycle distribution and apoptosis

48 h after lentiviral infection, cells were trypsinized and washed. For cell cycle analysis, cells were fixed in 95% ethanol at −4 °C overnight and then were stained using 50 μg/ml Propidium Iodide (PI) (Santa Cruz Biotechnology, Santa Cruz, CA, USA) for 30 min for apoptosis assessment. Then, cells collected were centrifugated for 5 minutes at 2,000rpm and resuspended in 1× binding buffer containing FITC-labeled Annexin V (25ng/ml) and propidium iodide (50ng/ml) (FITC Annexin V Apoptosis detection kit I, BD Pharmingen, San Jose, CA, USA). Then, the samples were immediately analyzed by flow cytometry with a BD FACSCanto II flow cytometer (BD Biosciences) at a low flow rate. Results were quantified with BD FACSDiva software v8.0 (Franklin Lakes, NJ BD Biosciences). A minimum of 10,000 events were gated per sample.

Cell invasion assay

Briefly, 1×10^5 cells in serum-free EMEM were added to the upper chamber of the Matrigel-coated insert (Merck Millipore, Darmstadt, Germany), and 500 μL of DMEM containing 10% FBS was added to the lower chamber for culture. The cells were cultured in a cell incubator for 24 h. Then, non-invading cells were removed and invading cells were fixed with 4% paraformaldehyde for 30 minutes and stained using 0.5% crystal violet (Sigma-Aldrich, St Louis, MO, USA) for 20 minutes. The invading cells were counted using an inverted microscope (Olympus, Tokyo, Japan).

Wound healing assay

24 h after lentiviral infection, 5×10^5 cells were seeded into 6-well culture plates and cultured to 90% confluence. Then, a sterile 200-μl micropipette tip was utilized to scratch the cell monolayer. The cells were further cultured in serum-free medium incubated in a cell incubator for another 48 h. Then, wound healing area was captured using an inverted microscope (Olympus) at a magnification of 200× and quantified using ImageJ software (1.8.0) (National Institutes of Health).

RNA Pull-Down Assay and Mass Spectrometry

PTTG3P and its antisense RNA were chemically synthesized and were inserted into the sites between KpnI and SacI in pBluescript II SK+. Biotin-labelled *PTTG3P* was first transcribed *in vitro* using Biotin RNA Labeling Mix (Roche, Germany) by T3 (for antisense)/T7 (for sense) RNA polymerase Mix (Roche Diagnostics, Indianapolis, IN, USA) according to the manufacturer's instructions. Then, the RNA products were treated with RNase-free DNase I (Roche) and purified with a RNeasy Mini Kit (Qiagen, Valencia, CA, USA). Total proteins extracted from Hep3B cells were then mixed with biotinylated RNA, incubated with Dynabeads Myone Streptavidin T1 beads (Invitrogen, Carlsbad, CA), and washed. The proteins binding to the streptavidin-coupled dynabeads were resolved by SDS-PAGE and visualized by silver staining. The specific bands were excised and analyzed by a linear ion trap-orbitrap mass spectrometer (LTQ-Orbitrap Velos, Thermo Fisher Scientific) coupled with a nanoflow LC system (Dina-2A, KYA Technologies). The proteins with Score Sequest HT > 6 were selected.

Western blot analysis

HCC cells were lysed on ice in RIPA buffer supplemented with protease inhibitors. Protein samples were separated on a 10% sodium dodecyl sulfate-polyacrylamide gel (SDS-PAGE), and then were electrotransferred onto polyvinylidene fluoride (Millipore) membranes. After that, the membranes were blocked in 5% non-fat milk powder for 2 h at room temperature and incubated with primary antibodies overnight at 4℃. After incubation with corresponding secondary antibodies conjugated to horseradish peroxidase, protein band signals were detected by BeyoECL Star Kit (Beyotime, Wuhan, China). Signal images were taken using a ChemiDoc imaging system (BIO-RAD, USA).

Real-Time Quantitative Reverse Transcription PCR (qRT-PCR)

qRT-PCR was conducted as described previously. In brief, total RNA was extracted from cell samples using TRIzol reagent (Thermo Fisher Scientific, Inc., Waltham, MA, USA). cDNAs were reversely transcribed with PrimeScript RT reagent kit (TaKara, Dalian, China). Then, qRT-PCR was conducted using a SYBR Premix Ex Taq Kit (TaKaRa, Dalian, China), with an Applied Biosystems 7500 Sequence Detection System (Applied Biosystem). Primer sequences for qRT-PCR were listed in (Supplementary Table 1). *GAPDH* expression was used as an internal control.

RNA immunoprecipitation (RIP) and Chromatin immunoprecipitation (ChIP)

RIP and ChIP assays were conducted using the EZ-Magna RIP™ RNA-Binding Protein Immunoprecipitation Kit (Merck Millipore) and EZ-Magna ChIP™ A/G Chromatin Immunoprecipitation Kit (Merck Millipore), respectively, according to the manufacturer's instruction.

In brief, Hep3B cells were lysed using RIPA buffer. For RIP, whole-cell lysate was incubated with the RIP immunoprecipitation buffer containing protein A/G magnetic beads coated with ILF2 or ILF3 antibody. Normal mouse IgG was used as the control. After being incubated for 2 h at 4°C, the precipitated RNA fraction was isolated and subjected to qRT-PCR analysis of *PTTG3P* expression.

For ChIP, the protein-DNA cross-links were collected and sonicated to an average size of 500~1000 bp. The chromatin was immunoprecipitated with mouse anti-ILF2 (ab154791, Abcam, Cambridge, UK) or mouse IgG overnight at 4 °C. Then, Immunoprecipitated DNA collected was performed by the EZ-Magna ChIP A/G Kit. The primers for ChIP-qPCR were provided in Supplementary Table 1.

RNA-seq

Total RNA was extracted from Hep3B cells 48 h after lentiviral mediated *PTTG3P* overexpression and subjected to RNA-seq study. RNA-Seq, data generation and normalization were conducted on the Illumina Cluster Station and Illumina Nova-seq 6000 System at Gene denovo Corp. (Guangzhou, China).

IHC staining

IHC staining data are both from the Human Protein Atlas (https://www.proteinatlas.org/) [23] and from our lab. For IHC of ENO2 expression in HCC tissues, a human HCC tissue array was obtained from Taibosi Bio (Xian, China). IHC staining was automatically conducted using BOND-III Automated IHC Stainer for Immunostaining (Leica Biosystems, Buffalo Grove, IL, USA). Primary anti-ENO2 (55235-1-AP) was purchased from Proteintech (Wuhan, China). Hematoxylin was used for counterstaining.

Immunofluorescent (IF) staining

Hep3B and HepG2 cells were grown on coverslips and infected for *PTTG3P* depletion. 24 h later, the cells were fixed in 4% paraformaldehyde, permeabilized, and blocked. Then, the coverslips were incubated with mouse anti-ILF2 (ab154791) and rabbit anti-ILF3 (19887-1-AP, Proteintech) at 4℃ overnight. Then the coverslips were washed and incubated with secondary anti-mouse IgG (Alexa Fluor 594, ab150116, Abcam) and anti-rabbit IgG (Alexa Fluor 488, ab150077, Abcam). Nuclear was stained by DAPI. Immunofluorescent staining was visualized using a fluorescence microscope (Olympus IX83).

Dual-luciferase assay

The full-length wild-type (WT) *TOP2A* promoter sequence and mutant sequences (with mutations of the potential ILF2/ILF3 binding motif) were chemically synthesized and cloned into the sites between KpnI and HindIII in the pGL3 basic vector (Promega, Madison, WI, USA). HCC cells were plated in 24-well plates at a density of 2×10^5 cells per well and were infected with lentivirus carrying sh*PTTG3P* alone or in

combination with sh*ILF2.* 24h later, cells were transfected with 1 μg of recombinant plasmids and 0.05 μg of pRL-CMV vector, using Lipofectamine 2000 (Invitrogen). 24 h after transfection, cells were lysed for the measurement of firefly luciferase and renilla luciferase activities, using a dual-specific luciferase assay kit (#E1910, Promega).

Animal study

Briefly, five-week-old male BALB/c nude mice were purchased from Chengdu Dashuo Experimental Animal Co., Ltd (Sichuan, China). $5*10^6$ Hep3B cells with *PTTG3P* overexpression, *PTTG3P* knockdown, or *TOP2A* knockdown were subcutaneously into the left or right flanks of mice. Tumor growth was recorded twice a week. Four weeks after, all mice were euthanatized. Tumors were excised, pictured and then, fixed and embedded in paraffin. Paraffin sections were applied for immunohistochemistry (IHC) staining of Ki-67 and IF staining of Terminal deoxynucleotidyl transferase dUTP nick end labeling (TUNEL). The experiment protocol was approved by the Animal Care and Use Committee of the University of Electronic Science and Technology of China.

Statistical analysis

Data analysis was performed using GraphPad Prism 8.1.2 (GraphPad Inc., La Jolla, CA, USA). One-way ANOVA with post hoc Tukey's multiple comparisons test was performed for comparison among three or more groups. For two-group comparisons, Welch's unequal variances *t*-test was conducted. Kaplan-Meier survival curves were generated by median gene expression, with Log-rank test to check differences. Pearson's coefficients were calculated to estimate correlation. $p < 0.05$ was considered to be statistically significant.

Results

PTTG3P upregulation is associated with enhanced proliferation and cell-cycle progression of HCC

To validate the dysregulation of *PTTG3P* in HCC, we retrospectively reviewed its expression in 10 databases with *PTTG3P* expression data in HCCDB, a database of HCC expression atlas [24]. *PTTG3P* upregulation is observed in 8/10 datasets (Fig. 1A). Notably, HCCDB15 refers to TCGA-LIHC. By RNA-FISH assay, we confirmed the cytoplasmic distribution of *PTTG3P* in Hep3B and HepG2 cells (Fig. 1B). To explore the functional role of *PTTG3P*, we designed *PTTG3P* shRNA and overexpression lentivirus (Fig. 1C-D). *PTTG3P* knockdown slowed HCC cell proliferation (Fig. 1E-F), increased G1 phase accumulation, and decreased the proportion of cells in the S phase (Fig. 1G-I). In comparison, *PTTG3P* overexpression significantly enhanced cell proliferation (Fig. 1E-F), decreased G1 phase accumulation but increased the ratio of cells in the S phase (Fig. 1G-I).

PTTG3P upregulation reduces apoptosis and enhances invasion and migration of HCC cells

By performing Annexin V/PI staining, we found that *PTTG3P* depletion led to increased cell apoptosis. In contrast, its overexpression resulted in reduced cell apoptosis (Fig. 2A-C). Matrigel invasion and scratch assays showed that *PTTG3P* knockdown impaired HCC cell invasion (Fig. 2D-F) and migration (Fig. 2G-I). However, its overexpression significantly enhanced cell invasion (Fig. 2D-F) and migration (Fig. 2G-I).

PTTG3P physically interacts with ILF2 and ILF3 in HCC

To investigate the functional role of *PTTG3P* in HCC, we tried to identify its interacting proteins. The schematic map showing the construction of recombinant pBluescript II SK + plasmid is presented in Fig. 3A. Then, RNA pull-down assay was conducted using Biotin-labelled sense *PTTG3P* and antisense *PTTG3P* followed by silver staining (Fig. 3B). The bands specific to *PTTG3P* were excised and subjected to mass spectrometry (Fig. 3B, Supplementary Table 2). Results showed that ILF3 (also known as NF90, 90 kD) has the highest Sequest HT score (Fig. 3C). This protein usually forms a regulatory complex with ILF2 (also known as NF45, 45 kD), which is also observed in the MS results (Fig. 3C). Sense *PTTG3P* specific 45 kD and 90 kD bands were also observed (Fig. 3D). Then, RNA-IP assay was conducted using anti-ILF2 and anti-ILF3, respectively. The presence of ILF2 and ILF3 in the anti-ILF2 and anti-ILF3 immunoprecipitated samples were confirmed by western blotting (Fig. 3E-F). These samples had significantly higher enrichment of *PTTG3P* compared to the IgG control group (Fig. 3G).

By checking RNA-seq and survival data in TCGA-LIHC and RNA-seq data from GTEx, we confirmed the upregulation of *ILF2* and *ILF3* in HCC tissues compared to normal liver and tumor-adjacent normal tissues (Fig. 3H). Survival analysis confirmed the association between upregulated *ILF2/ILF3* and unfavorable prognosis (Fig. 3I-L).

PTTG3P depletion increases the binding of ILF2 to the promoter of TOP2A

Since we characterized that *PTTG3P* interacts with ILF2 and ILF3 in HCC, while the ILF2/ILF3 complex as a transcriptional enhancer/factor, we tried to explore their downstream targets in common. Firstly, we overexpressed *PTTG3P* in Hep3B cells. 48 h later, total RNA was extracted for RNA-seq. By setting adj. $p < 0.05$ and log 2(Fold Change, FC) ≥ 1 as the cutoff, we identified 215 dysregulated genes (Supplementary Table 3). One recent study explored dysregulated genes in HepG2 cells after ILF2 depletion [25]. Using their data, we identified 125 genes downregulated after ILF2 inhibition (adj.$p < 0.05$ and log 2(FC) ≤ -1) (Supplementary Table 4). These two sets shared six genes, including *TOP2A*, *KIF14*, *BUB1*, *SERPINA3*, *STRA6*, and *KREMEN1* (Fig. 4A). For validation purposes, we further assessed the correlation of these genes with *PTTG3P* and *ILF2* in TCGA-LIHC (Fig. 4B). By setting moderate correlations as the cutoff (| Pearson's r ≥ 0.4,| adj. $p < 0.05$), we found that *TOP2A*, *KIF14*, and *BUB1* as potential candidates. Besides, we manually added *LOXL2* and *ENO2*, two overexpressed genes after *PTTG3P* overexpression (Supplementary Table 3), as potential candidates.

We conducted ChIP-qPCR assay to check whether *PTTG3P* depletion alters the binding of ILF2 to the promoter of these genes. Results showed that after *PTTG3P* knockdown, ILF2 presented enhanced binding to the promoter of *TOP2A*, but showed weakened binding to the promoter of *ENO2* (Fig. 4C-D). By

checking protein level expression, we observed negative ENO2 expression in both normal liver and HCC tissues (Fig. 4E). In consistence with previous reports, we confirmed negative *TOP2A* expression in hepatocytes in normal liver (all negative by three primary antibodies in the HPA, HPA006458, HPA026773, and CAB002448) (Fig. 4F, green frame). In comparison, medium to high TOP2A expression was observed in HCC tissues (Fig. 4F, brown frame).

PTTG3P inhibition results in nuclear translocation of ILF2

After *PTTG3P* depletion, we observed nuclear accumulation of ILF2 by IF staining (Fig. 5A). However, no alteration was observed in the cellular distribution of ILF3 (Fig. 5A). Colocalization of ILF2 and ILF3 was observed in both cytoplasma and nuclear (Fig. 5A). By performing fractional western blotting, we confirmed this distributional alteration (Fig. 5B).

Via scanning the promoter region of *TOP2A*, we observed two potential ILF2/ILF3 binding sites (Fig. 5C). Then, we generated luciferase reporter plasmids carrying wild-type (pGL3-TOP2A-WT) and mutant TOP2A promoter sequences (pGL3-TOP2A-MT1, pGL3-TOP2A-MT2, and pGL3-TOP2A-MT3) based on a pGL3-basic backbone. *ILF2* inhibition significantly reduced the luciferase activity of the reporters carrying at least one wild-type ILF2/ILF3 binding site (Fig. 5D-F), but had no influence on the reporter with two mutant sites (Fig. 5G). In contrast, *PTTG3P* inhibition significantly increased the luciferase activity of the reporters carrying at least one wild-type ILF2/ILF3 binding site (Fig. 5D-F), but did not influence the luciferase activity of the reporter with two mutant sites (Fig. 5G). These findings suggest that *PTTG3P* depletion might enhance *TOP2A* expression via promoting nuclear translocation of ILF2. To test this hypothesis, we checked the mRNA expression of *TOP2A* expression after *PTTG3P* knockdown. Interestingly, *PTTG3P* depletion did not increase but decreased *TOP2A* mRNA levels (Fig. 5H). This discrepancy implies that some other mechanisms are involved in regulating *TOP2A* expression/stability.

ILF2/ILF3 complex stabilizes TOP2A mRNA in the cytoplasm

Since the ILF2/ILF3 complex may act as an mRNA stabilizer, we tested whether ILF2/ILF3 binds to the 3'UTR of *TOP2A* mRNA and regulates its stability. RIP-qPCR confirmed significantly higher enrichment of *TOP2A* 3'UTR in the samples precipitated by anti-ILF2 than the IgG control (Fig. 6A-B). *PTTG3P* depletion significantly reduced the enrichment level (Fig. 6A-B). These findings suggest that ILF2 binds to the 3'UTR of *TOP2A* mRNA, the effect of which was enhanced by *PTTG3P*. ILF2 or *PTTG3P* depletion significantly reduced the stability of *TOP2A* mRNA (Fig. 6C-D), the effect of which was enhanced by simultaneous ILF2 and *PTTG3P* inhibition (Fig. 6C-D).

PTTG3P or TOP2A inhibition impairs HCC growth in-vivo

By generating Hep3B derived *in vivo* tumor model in mice, we found that *PTTG3P* overexpression significantly enhanced tumor growth (Fig. 7A-B). *PTTG3P* or *TOP2A* inhibition significantly slowed the growth rate (Fig. 7A-B). HE and TUNEL staining showed that *PTTG3P* and *TOP2A* inhibition are associated with enhanced tumor necrosis and apoptosis (Fig. 7C, top and bottom panels). In agree with

these data, Ki-67 staining indicated a decreased level of cell proliferation in both *PTTG3P* KD and *TOP2A* KD groups (Fig. 7C, middle panel).

Based on these findings, we infer that *PTTG3P* exerts dual-regulation in *TOP2A* expression at both transcriptional and post-transcriptional levels. It is usually overexpressed in HCC tumor cells and accumulated in cytoplasm. Under this circumstance, it forms a complex with ILF2/ILF3, which binds to the 3'UTR of *TOP2A* mRNA and increases its stability. However, *PTTG3P* depletion can trigger nuclear translocation of ILF2, which binds to the promoter of the *TOP2A* gene and enhances its transcription (Fig. 8).

Discussion

PTTG3P has been demonstrated as an oncogenic lncRNA in multiple other cancers, such as gastric cancer [26], colorectal cancer [27], head and neck squamous cell carcinoma [28], and cervical cancer [29]. Previous studies found that the regulatory effects of PTT3GP are quite complex. It can act as a miRNA sponge [14,27] and a functional partner of transcriptional factor [15]. In the current study, we confirmed that *PTTG3P* overexpression contributed to enhanced proliferation, cell-cycle progression, invasion, and migration of HCC. Then, we found that *PTTG3P* interacts with both ILF2 and ILF3 in HCC cells. The association between ILF2/ILF3 upregulation and the unfavorable prognosis was also confirmed based on survival data from TCGA-LIHC.

ILF2/ILF3 complex can act as an mRNA stabilizer via binding to the 3'UTR of a cluster of mitotic mRNAs (including *NUF2*, *CDK1*, *CCNE1*, *CCNA2*, and *BIRC5*) and reduce Staufen-mediated mRNA decay [21,25]. However, the spectrum of mRNAs controlled by the ILF2/ILF3 complex and other modulators of this complex has not been well characterized. In this study, we revealed that the binding between *PTTG3P* and ILF2 helps maintain the cytoplasmic distribution of ILF2. Together with ILF2, *PTTG3P* binds to the 3'UTR of TOP2A. *PTTG3P* depletion impairs the binding ability and reduces *TOP2A* mRNA stability.

Similar to our reports, some recent studies also reported the binding of lncRNAs to ILF2/ILF3. LncRNA *DANCR* interacts with ILF2/ILF3 complex and increases *HIF1A* mRNA stability in nasopharyngeal carcinoma [30]. LINC00470 forms a complex with ILF2/ILF3 and enhances its interaction with *CCNE1* mRNA, which further enhances its stability and facilitates cell-cycle progression in HCC [31]. LncRNA AK085865 specifically interacts with ILF2 and negatively regulates the ILF2/ILF3 complex-mediated miRNA-192 biogenesis in bone marrow-derived macrophages [32]. These findings suggest that lncRNAs can act as an important functional modulator of the ILF2/ILF3 complex.

TOP2A is a protein regulating the topological state of DNA during transcription via transiently breaking and rejoining DNA strands. As a critical nuclear enzyme for DNA replication- and cell division-regulating, TOP2A exerts multiple functions across the cell cycle, and its overexpression is a critical driver of

malignant transformation and uncontrolled proliferation of tumor cells [33,34]. Multiple anti-drugs targeting TOP2A, such as mitoxantrone, mAMSA, etoposide, doxorubicin, epirubicin, and idarubicin, have been developed [35]. *TOP2A* overexpression is associated with early age onset, shorter survival, and chemoresistance to doxorubicin of HCC [36,37]. Depletion of *TOP2A* significantly suppresses the proliferation of HCC cells [38], suggesting that TOP2A is an important therapeutic target in HCC.

Since PTTG3P is usually aberrantly upregulated in HCC, its accumulation in the cytoplasm make it mainly act as a *TOP2A* stabilizer. Therefore, when it is knocked down, we observed downregulated *TOP2A* mRNA levels. After *PTTG3P* depletion, we observed nuclear accumulation of ILF2 and increased binding of ILF2 to the promoter region of *TOP2A*. Dual-luciferase assay confirmed that ILF2 could activate the *TOP2A* promoter, suggesting that the ILF2/ILF3 complex acts as a transcriptional enhancer of *TOP2A*. The translation of ILF2 to the nuclear part might be utilized by HCC cells to compensate the loss of *PTTG3P* and associated *TOP2A* instability. These mechanisms help explain why *PTTG3P* depletion does not lead to drastically downregulated *TOP2A* mRNA levels.

In conclusion, this study identified *PTTG3P* as a novel functional partner of the ILF2/ILF3 complex, which enhances the binding of the ILF2/ILF3 complex to the 3'UTR of *TOP2A* mRNA and increases its stability in HCC. When it is overexpressed in HCC tumor cells, it mainly acts as a *TOP2A* mRNA stabilizer. *PTTG3P* depletion results in nuclear accumulation of ILF2, which binds to the promoter of *TOP2A* and enhances its transcription. These findings help expand our understanding of the oncogenic mechanisms of *PTTG3P* in HCC.

Declarations

Acknowledgment

The authors have no conflict of interest.

Authors' contributions

TL,MZ,HSB conceived the idea; HYZ,JHL performed the analysis; HYJ,LL interpreted the results and made tables. All authors read and approved the final manuscript

Funding

none

Availability of data and materials

the datasets used during the study are available from the corresponding authors on reasonable request

Ethics approval and consent to participate

all animal procedures and care were conducted by institutional guidelines and in compliance with national and international laws and policies

Consent for publication

not applicable

Competing interests

the authors declare that they have no competing interests

References

1. Bhan A, Soleimani M, Mandal SS. Long Noncoding RNA and Cancer: A New Paradigm. *Cancer Res.*2017;77(15):3965-3981.
2. Huang Z, Zhou JK, Peng Y, He W, Huang C. The role of long noncoding RNAs in hepatocellular carcinoma. *Mol Cancer.*2020;19(1):77.
3. Lanzafame M, Bianco G, Terracciano LM, Ng CKY, Piscuoglio S. The Role of Long Non-Coding RNAs in Hepatocarcinogenesis. *Int J Mol Sci.*2018;19(3).
4. Mondal T, Subhash S, Vaid R, et al. MEG3 long noncoding RNA regulates the TGF-beta pathway genes through formation of RNA-DNA triplex structures. *Nat Commun.*2015;6:7743.
5. Cloutier SC, Wang S, Ma WK, et al. Regulated Formation of lncRNA-DNA Hybrids Enables Faster Transcriptional Induction and Environmental Adaptation. *Mol Cell.*2016;62(1):148.
6. Xu W, Deng B, Lin P, et al. Ribosome profiling analysis identified a KRAS-interacting microprotein that represses oncogenic signaling in hepatocellular carcinoma cells. *Sci China Life Sci.*2020;63(4):529-542.
7. Jiang W, Cheng X, Wang T, Song X, Zheng Y, Wang L. LINC00467 promotes cell proliferation and metastasis by binding with IGF2BP3 to enhance the mRNA stability of TRAF5 in hepatocellular carcinoma. *J Gene Med.*2020;22(3):e3134.
8. Xu J, Lu Y, Liu Q, et al. Long noncoding RNA GMAN promotes hepatocellular carcinoma progression by interacting with eIF4B. *Cancer Lett.*2020;473:1-12.
9. Li D, Zhang J, Li J. Role of miRNA sponges in hepatocellular carcinoma. *Clin Chim Acta.*2020;500:10-19.
10. Hu X, Feng Y, Zhang D, et al. A functional genomic approach identifies FAL1 as an oncogenic long noncoding RNA that associates with BMI1 and represses p21 expression in cancer. *Cancer Cell.*2014;26(3):344-357.
11. Gou Q, Gao L, Nie X, et al. Long Noncoding RNA AB074169 Inhibits Cell Proliferation via Modulation of KHSRP-Mediated CDKN1a Expression in Papillary Thyroid Carcinoma. *Cancer Res.*2018;78(15):4163-4174.

12. Bai H, Luo X, Liao D, Xiong W, Zeng M, Zheng B. Long Noncoding RNA PTTG3P Expression Is an Unfavorable Prognostic Marker for Patients With Hepatocellular Carcinoma. *Technol Cancer Res Treat.*2019;18:1533033819887981.
13. Huang JL, Cao SW, Ou QS, et al. The long non-coding RNA PTTG3P promotes cell growth and metastasis via up-regulating PTTG1 and activating PI3K/AKT signaling in hepatocellular carcinoma. *Mol Cancer.*2018;17(1):93.
14. Zhou Q, Zhang W, Wang Z, Liu S. Long non-coding RNA PTTG3P functions as an oncogene by sponging miR-383 and up-regulating CCND1 and PARP2 in hepatocellular carcinoma. *BMC Cancer.*2019;19(1):731.
15. Shih JH, Chen HY, Lin SC, et al. Integrative analyses of noncoding RNAs reveal the potential mechanisms augmenting tumor malignancy in lung adenocarcinoma. *Nucleic Acids Res.*2020;48(3):1175-1191.
16. Shi L, Godfrey WR, Lin J, Zhao G, Kao PN. NF90 regulates inducible IL-2 gene expression in T cells. *J Exp Med.*2007;204(5):971-977.
17. Kiesler P, Haynes PA, Shi L, Kao PN, Wysocki VH, Vercelli D. NF45 and NF90 regulate HS4-dependent interleukin-13 transcription in T cells. *J Biol Chem.*2010;285(11):8256-8267.
18. Nakadai T, Fukuda A, Shimada M, Nishimura K, Hisatake K. The RNA binding complexes NF45-NF90 and NF45-NF110 associate dynamically with the c-fos gene and function as transcriptional coactivators. *J Biol Chem.*2015;290(44):26832-26845.
19. Mognol GP, Gonzalez-Avalos E, Ghosh S, et al. Targeting the NFAT:AP-1 transcriptional complex on DNA with a small-molecule inhibitor. *Proc Natl Acad Sci U S A.*2019;116(20):9959-9968.
20. Higuchi T, Todaka H, Sugiyama Y, et al. Suppression of MicroRNA-7 (miR-7) Biogenesis by Nuclear Factor 90-Nuclear Factor 45 Complex (NF90-NF45) Controls Cell Proliferation in Hepatocellular Carcinoma. *J Biol Chem.*2016;291(40):21074-21084.
21. Jiang W, Huang H, Ding L, et al. Regulation of cell cycle of hepatocellular carcinoma by NF90 through modulation of cyclin E1 mRNA stability. *Oncogene.*2015;34(34):4460-4470.
22. Chen X, He Y, Zhu Y, Du J, Sun H. linc-AAM Facilitates Gene Expression Contributing to Macrophage Activation and Adaptive Immune Responses. *Cell Rep.*2021;34(1):108584.
23. Uhlen M, Fagerberg L, Hallstrom BM, et al. Proteomics. Tissue-based map of the human proteome. *Science.*2015;347(6220):1260419.
24. Lian Q, Wang S, Zhang G, et al. HCCDB: A Database of Hepatocellular Carcinoma Expression Atlas. *Genomics Proteomics Bioinformatics.*2018;16(4):269-275.
25. Nourreddine S, Lavoie G, Paradis J, et al. NF45 and NF90 Regulate Mitotic Gene Expression by Competing with Staufen-Mediated mRNA Decay. *Cell Rep.*2020;31(7):107660.
26. Weng W, Ni S, Wang Y, et al. PTTG3P promotes gastric tumour cell proliferation and invasion and is an indicator of poor prognosis. *J Cell Mol Med.*2017;21(12):3360-3371.

27. Liu N, Dou L, Zhang X. LncRNA PTTG3P Sponge Absorbs microRNA-155-5P to Promote Metastasis of Colorectal Cancer. *Onco Targets Ther.*2020;13:5283-5291.
28. Grzechowiak I, Gras J, Szymanska D, et al. The Oncogenic Roles of PTTG1 and PTTG2 Genes and Pseudogene PTTG3P in Head and Neck Squamous Cell Carcinomas. *Diagnostics (Basel).*2020;10(8).
29. Guo XC, Li L, Gao ZH, Zhou HW, Li J, Wang QQ. The long non-coding RNA PTTG3P promotes growth and metastasis of cervical cancer through PTTG1. *Aging (Albany NY).*2019;11(5):1333-1341.
30. Wen X, Liu X, Mao YP, et al. Long non-coding RNA DANCR stabilizes HIF-1alpha and promotes metastasis by interacting with NF90/NF45 complex in nasopharyngeal carcinoma. *Theranostics.*2018;8(20):5676-5689.
31. Huang W, Liu J, Yan J, et al. LncRNA LINC00470 promotes proliferation through association with NF45/NF90 complex in hepatocellular carcinoma. *Hum Cell.*2020;33(1):131-139.
32. Zhang Y, Li X, Wang C, Zhang M, Yang H, Lv K. lncRNA AK085865 Promotes Macrophage M2 Polarization in CVB3-Induced VM by Regulating ILF2-ILF3 Complex-Mediated miRNA-192 Biogenesis. *Mol Ther Nucleic Acids.*2020;21:441-451.
33. Nielsen CF, Zhang T, Barisic M, Kalitsis P, Hudson DF. Topoisomerase IIalpha is essential for maintenance of mitotic chromosome structure. *Proc Natl Acad Sci U S A.*2020;117(22):12131-12142.
34. Ju BG, Lunyak VV, Perissi V, et al. A topoisomerase IIbeta-mediated dsDNA break required for regulated transcription. *Science.*2006;312(5781):1798-1802.
35. Lee KC, Bramley RL, Cowell IG, Jackson GH, Austin CA. Proteasomal inhibition potentiates drugs targeting DNA topoisomerase II. *Biochem Pharmacol.*2016;103:29-39.
36. Wong N, Yeo W, Wong WL, et al. TOP2A overexpression in hepatocellular carcinoma correlates with early age onset, shorter patients survival and chemoresistance. *Int J Cancer.*2009;124(3):644-652.
37. Panvichian R, Tantiwetrueangdet A, Angkathunyakul N, Leelaudomlipi S. TOP2A amplification and overexpression in hepatocellular carcinoma tissues. *Biomed Res Int.*2015;2015:381602.
38. Kwan SY, Sheel A, Song CQ, et al. Depletion of TRRAP Induces p53-Independent Senescence in Liver Cancer by Down-Regulating Mitotic Genes. *Hepatology.*2020;71(1):275-290.

Figures

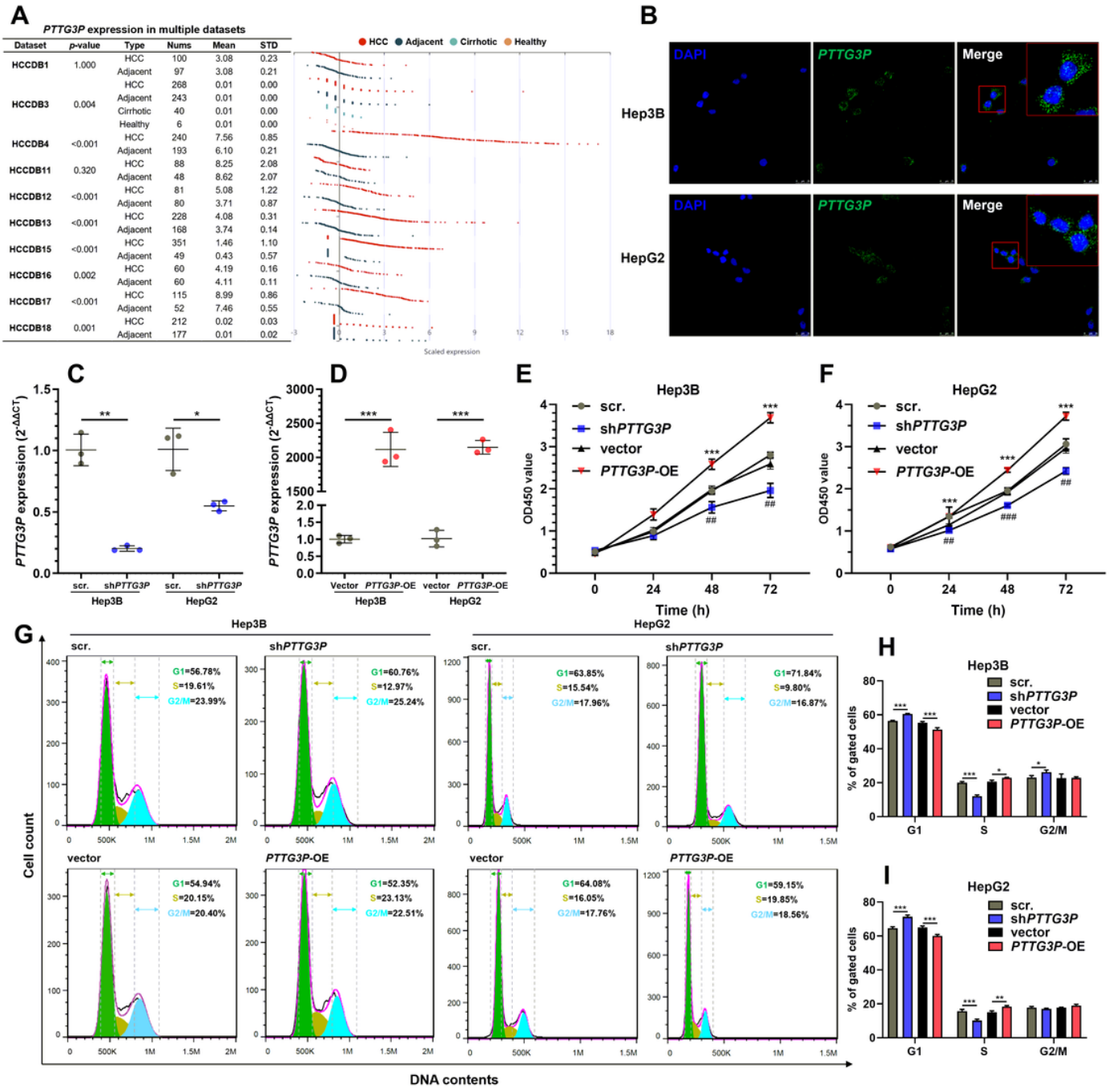

Figure 1

PTTG3P upregulation is associated with enhanced proliferation and cell-cycle progression of HCC

A. Data summary (left) and plot charts (right) comparing *PTTG3P* expression in 10 datasets collected in HCCDB (http://lifeome.net/database/hccdb/home.html). **B.** RNA-FISH assay was performed to visualize the presence of *PTTG3P* (green) in Hep3B and HepG2 cells. **C-D.** qRT-PCR analysis of *PTTG3P* expression in Hep3B and HepG2 cells, 24 h after lentiviral mediated *PTTG3P* knockdown or overexpression (OE). **E-F.** CCK-8 assay of Hep3B (D) and HepG2 (E) cell proliferation at the indicating points. Cell treatments were

as indicated in panel B-C. **G-HI.** Representative images (G) and quantitation (H-I) of flow cytometric analysis of cell cycle distribution. Cell treatments were as indicated in panel C-D.

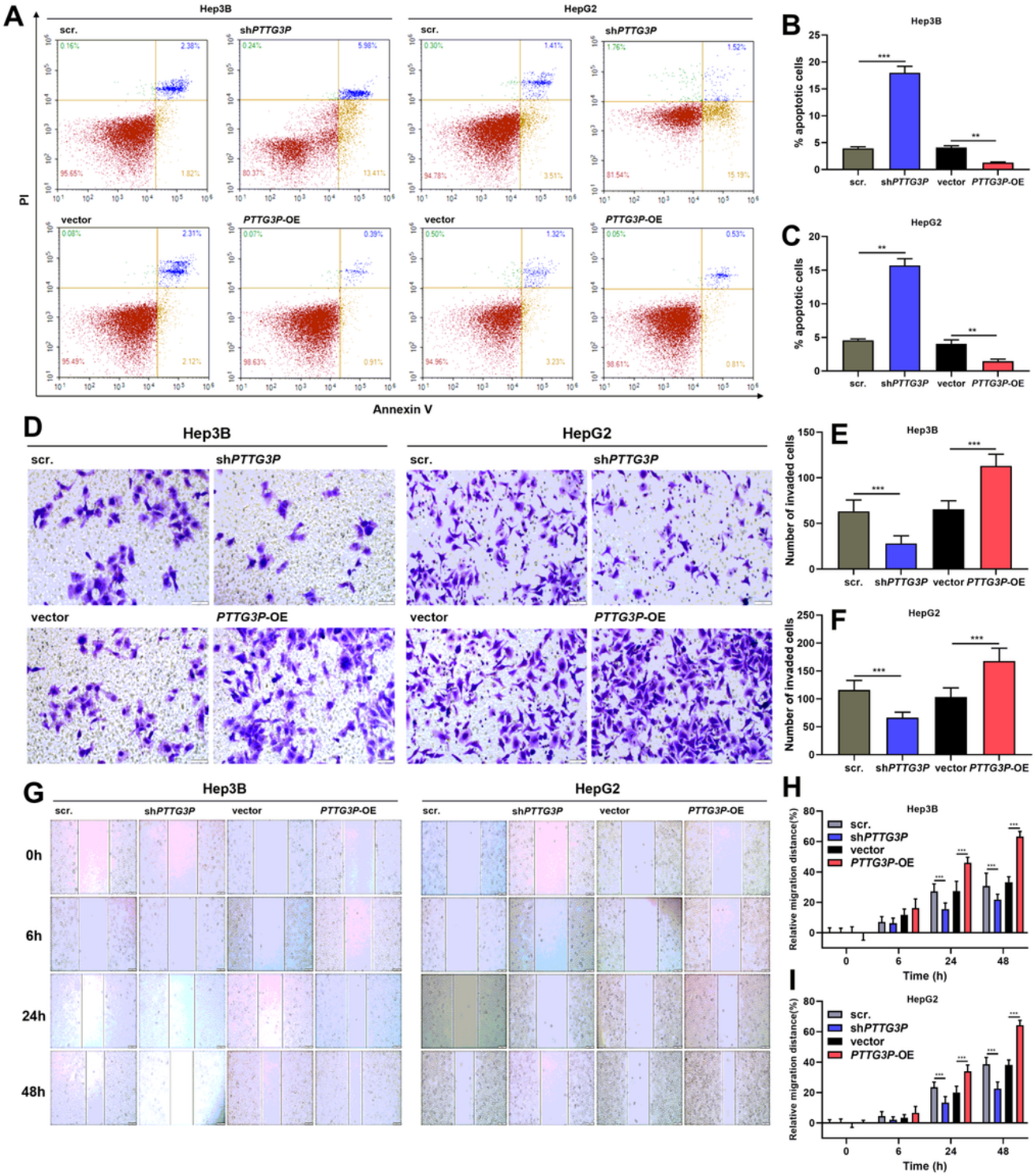

Figure 2

PTTG3P upregulation reduces apoptosis and enhances invasion and migration of HCC cells

A-C. Representative images (A) and quantitation (B-C) of flow cytometric analysis of Annexin V/PI staining of Hep3B and HepG2 cells 48 h after lentiviral mediated *PTTG3P* knockdown or overexpression. **D-I.** Representative images (D and G) and quantitation (E-F, H-I) of migration invasion assay (D-F) and scratch assay (G-I) of Hep3B and HepG2 cells 48 h after lentiviral mediated *PTTG3P* knockdown or overexpression.

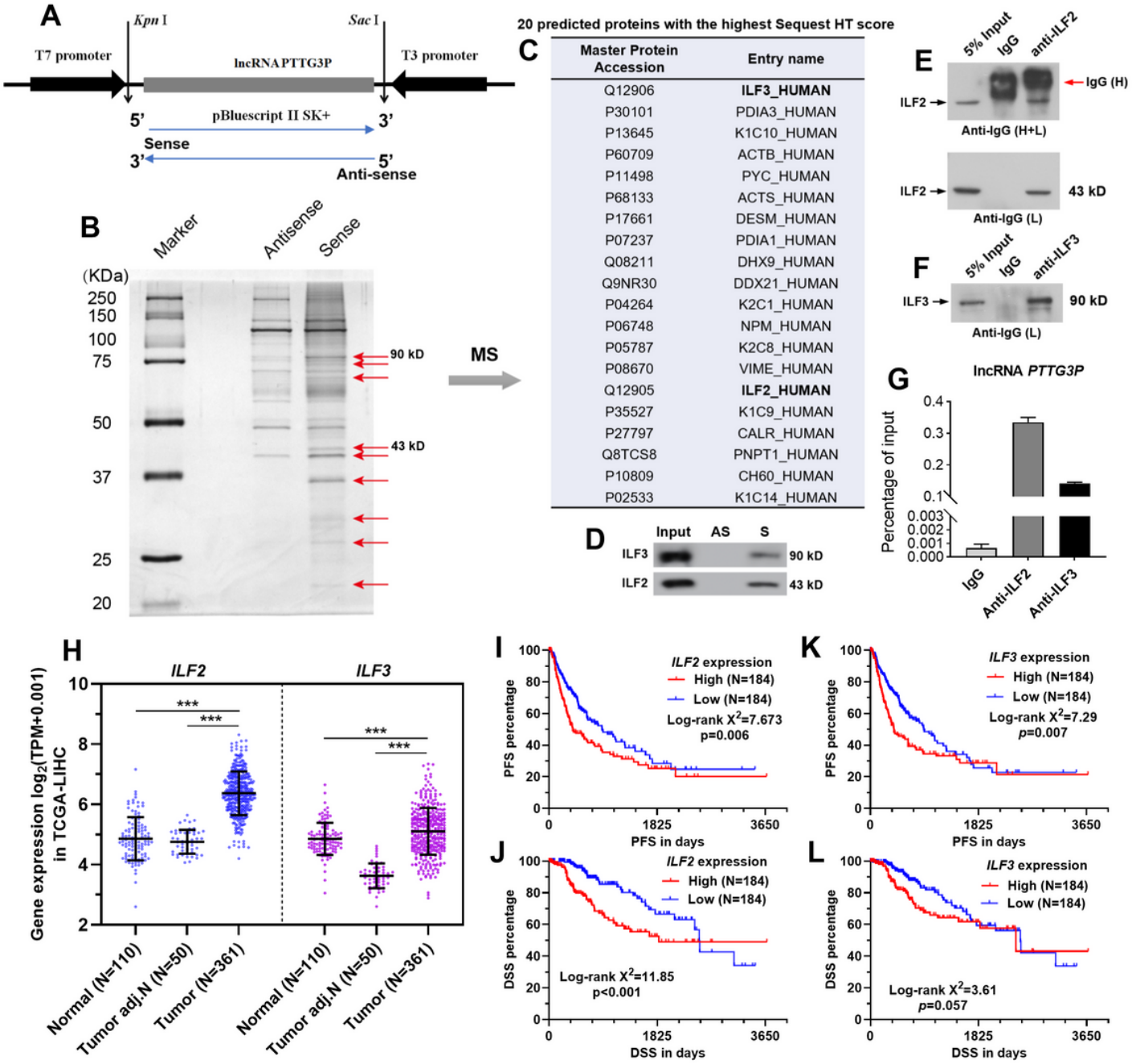

Figure 3

PTTG3P physically interacts with ILF2 and ILF3 in HCC

A. A schematic map showing the construction of recombinant pBluescript II SK+ plasmid carrying sense and antisense *PTTG3P*. **B.** SDS-PAGE of proteins purified from RNA pull-down assay using biotinylated *PTTG3P* or antisense RNA in Hep3B cells were visualized by silver staining. The highlighted protein bands (indicated by red arrows) were excised for MS analysis. **C.** A summary table listing the top 20 inferred proteins (with the highest Sequest HT Score) from LS-MS. **D.** Western blot analysis of the specific association of ILF2, ILF3 and lncRNA-*PTTG3P*. GAPDH was used as a negative control. AS: antisense strand of *PTTG3P*, S: sense strand of *PTTG3P*. **E-F.** Western blot analysis of the presence of ILF2 (E) and ILF3 (F) in the anti-ILF2 and anti-ILF3 immunoprecipitated Hep3B cell lysate. For ILF2 group, representative images of ILF2 detected by secondary anti-IgG (H/L) (up) and anti-IgG (L) (down) were provided. **G.** qRT-PCR analysis was performed to detect the enrichment of *PTTG3P* in the anti-ILF2 and anti-ILF3 immunoprecipitated samples. Relative enrichment was presented as the percentage of input. **H.** Plot chart showing the expression of *ILF2* and *ILF3* in TCGA-LIHC and GTEx. **I-L.** K-M survival analysis of PFS (I and K) and DSS (J and L) in HCC cases in TCGA-LIHC. Patients were separated into two groups by median *ILF2* (I-J) or *ILF3* (K-L) expression.

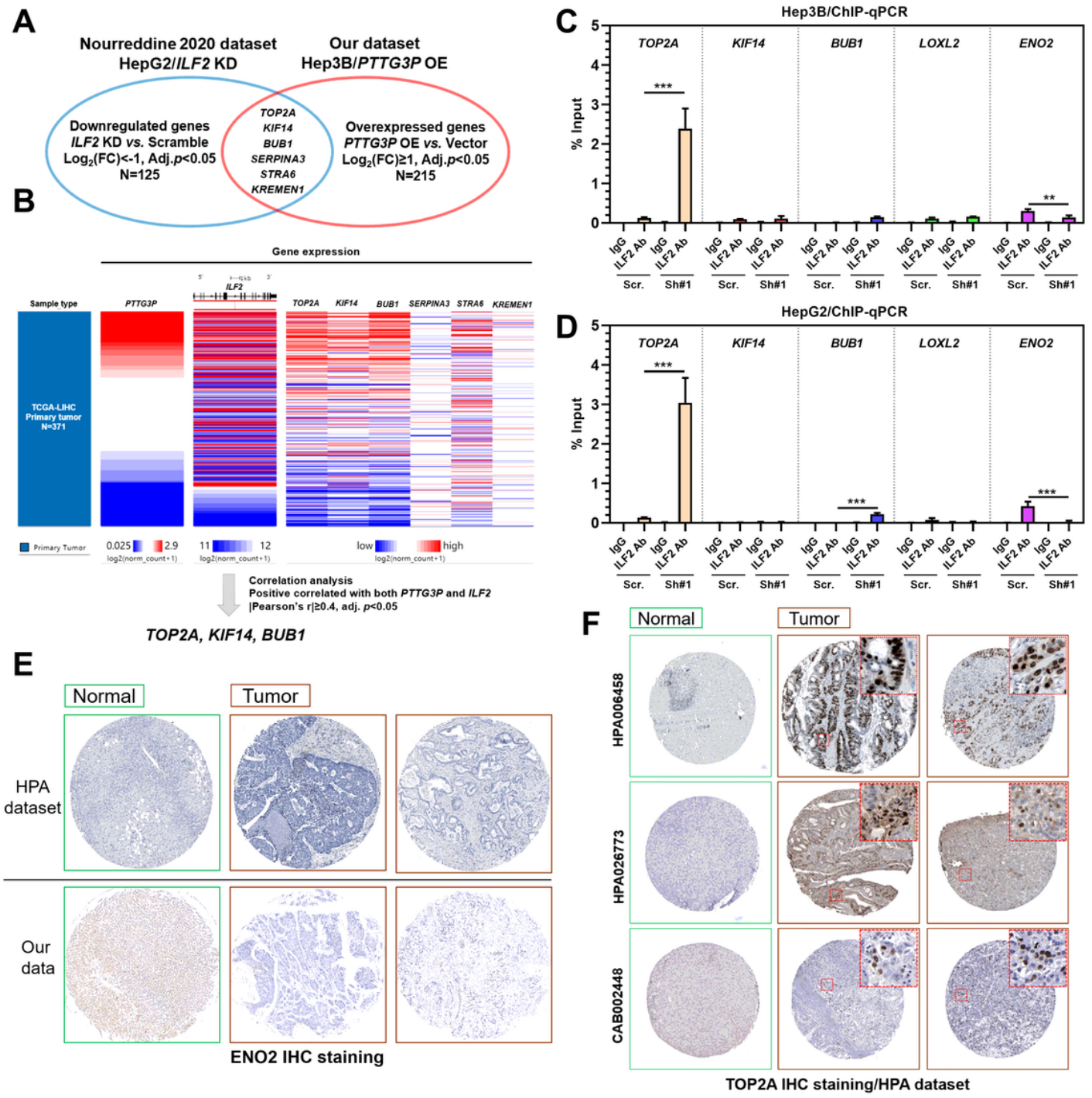

Figure 4

PTTG3P depletion increases the binding of ILF2 to the promoter of *TOP2A*

A. Screening of the potential downstream genes of *PTTG3P* and *ILF2* in common. The overlapping subset (N=6) of Nourreddine 2020 dataset and our own RNA-seq was identified. **B.** A heatmap showing the correlation of the candidate genes identified in the panel A with *PTTG3P* and *ILF2* in TCGA-LIHC. **C-D.** ChIP-qPCR analysis was conducted the Hep3B (C) and HepG2 (D) cells with or without *PTTG3P*

depletion. Anti-ILF2 (ILF2 Ab) or control IgG was used for IP. Then, the enrichment of the promoter segments of the candidate genes (*TOP2A, KIF14, BUB1, LOXL2,* and *ENO2*) in the precipitated samples were assessed by qPCR. The relative enrichment was presented as % input. **E-F.** IHC staining of ENO2 and TOP2A expression in normal liver and HCC tissues. Image credit: the HPA. The images obtained from the HPA can be accessed via:

https://www.proteinatlas.org/ENSG00000111674-ENO2/tissue/liver

https://www.proteinatlas.org/ENSG00000111674-ENO2/pathology/liver+cancer

https://www.proteinatlas.org/ENSG00000131747-TOP2A/tissue/liver

And https://www.proteinatlas.org/ENSG00000131747-TOP2A/pathology/liver+cancer

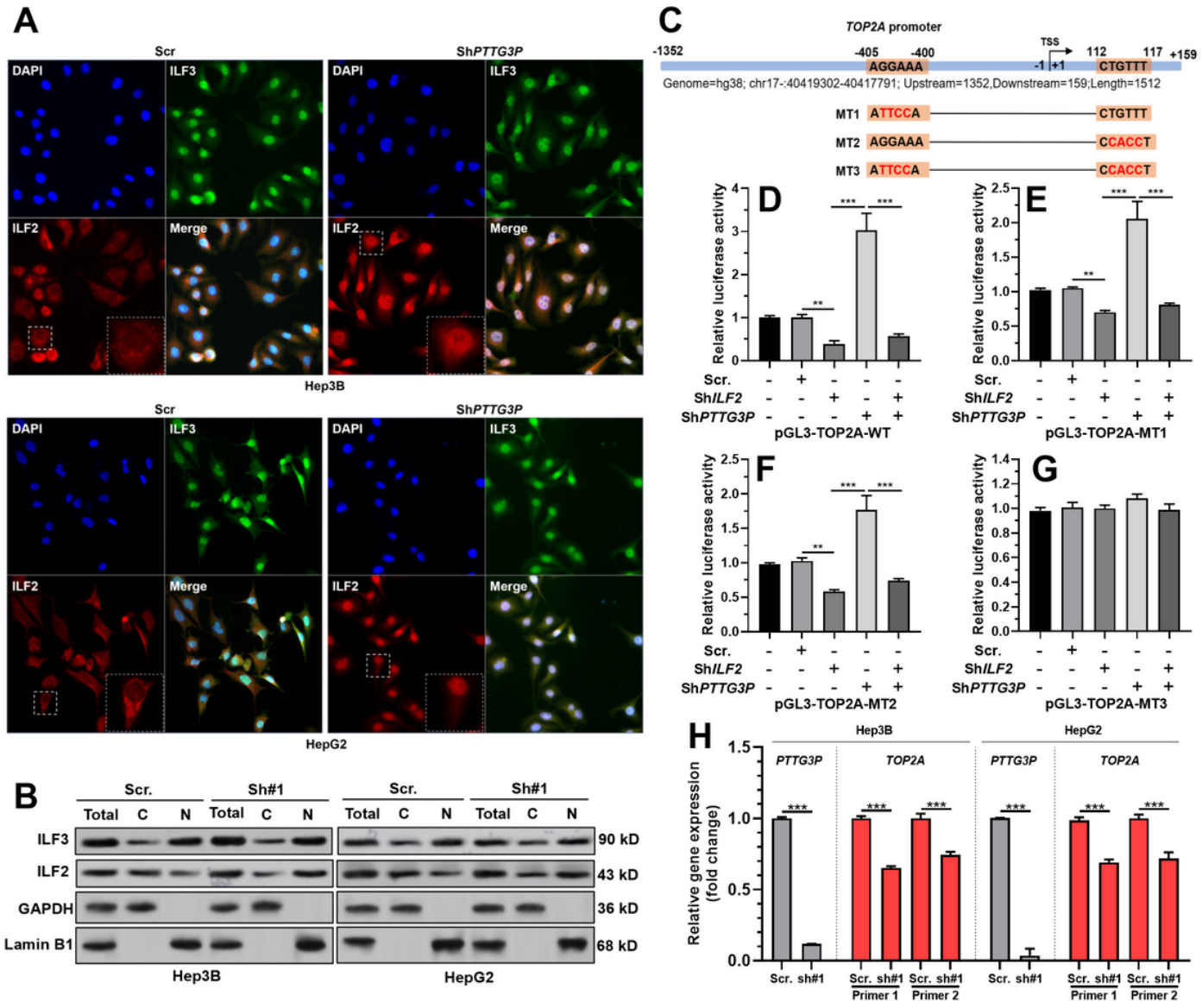

Figure 5

PTTG3P inhibition resulted in nuclear translocation of ILF2

A. IF staining of ILF2 (red) and ILF3 (green) expression in Hep3B (up) and HepG2 (down) cells with or without *PTTG3P* depletion. **B.** Western blot analysis of ILF2 and ILF3 expression in the cytoplasm (C) and nuclear (N) part in Hep3B (left) and HepG2 (right) cells with or without *PTTG3P* depletion. **C.** Predicted binding site of ILF2/ILF3 complex in the promoter region of *TOP2A.* D-G. Dual-luciferase assay was conducted to assess the relative luciferase activity of the recombinant plasmids carrying wild-type (pGL3-TOP2A-WT) or mutant TOP2A promoter sequences (pGL3-TOP2A-MT1, pGL3-TOP2A-MT2, and pGL3-TOP2A-MT3) in Hep3B cells with ILF2 or *PTTG3P* depletion or with *ILF2* and *PTTG3P* depletion simultaneously. **H.** qRT-PCR analysis of *TOP2A* mRNA expression in Hep3B (left) and HepG2 (right) cells with or without *PTTG3P* depletion.

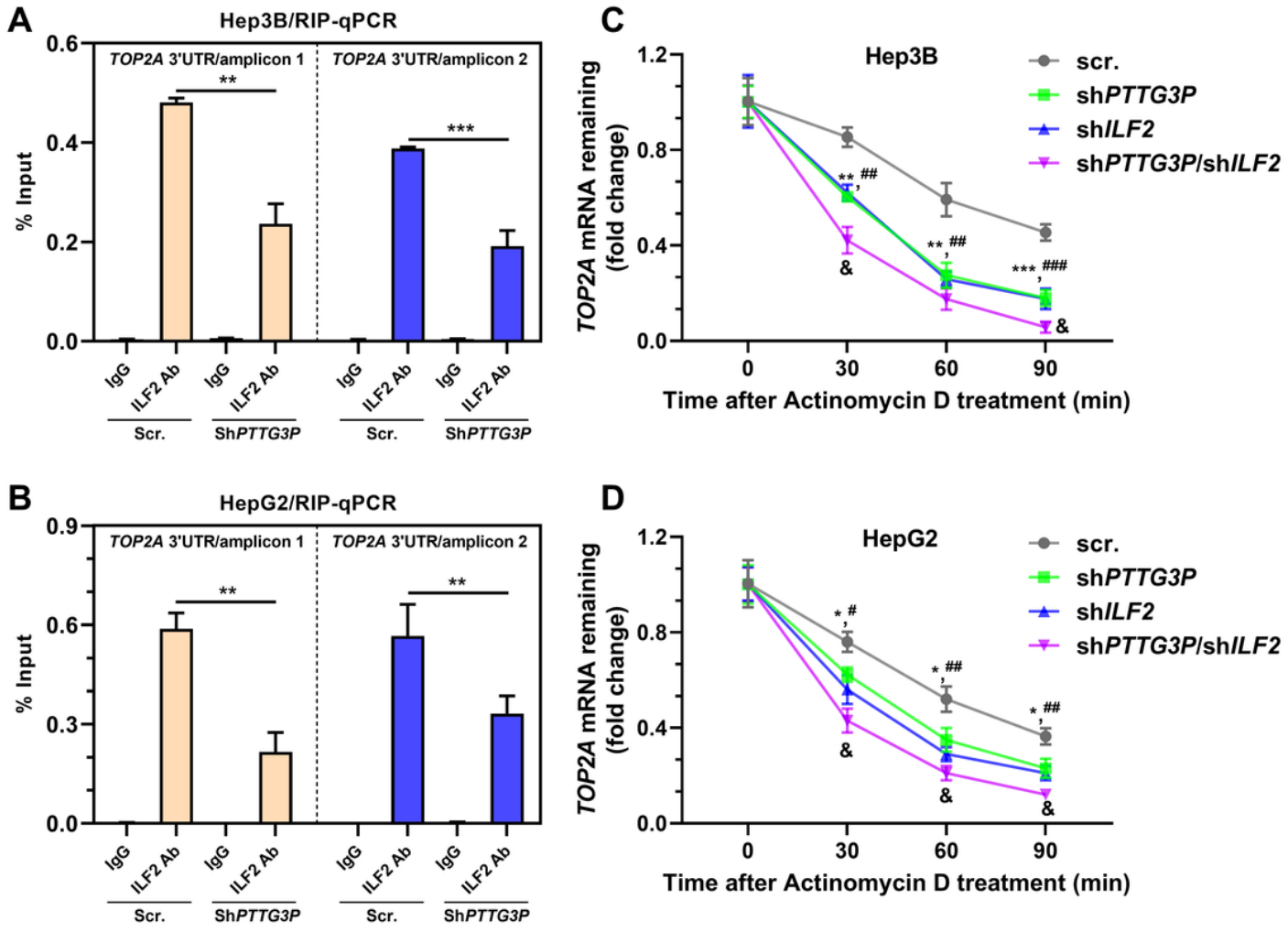

Figure 6

ILF2/ILF3 complex stabilizes *TOP2A* mRNA in the cytoplasm

A-B. RIP-qPCR analysis was conducted in Hep3B (A) and HepG2 (B) cells to assess the binding of ILF2 to the 3'UTR of *TOP2A* mRNA. Hep3B and HepG2 were subjected to lentivirus-mediated *PTTG3P* depletion. Anti-ILF2 (ILF2 Ab) or control IgG was used for IP. Then, the enrichment of *TOP2A* mRNA 3'UTR segment in the precipitated samples was assessed by qPCR. The relative enrichment was presented as % input. **C-D.** Quantification of *TOP2A* mRNA in Hep3B (C) and HepG2 (D) cells at the indicated time points after actinomycin D (6 μg/ml) treatment.

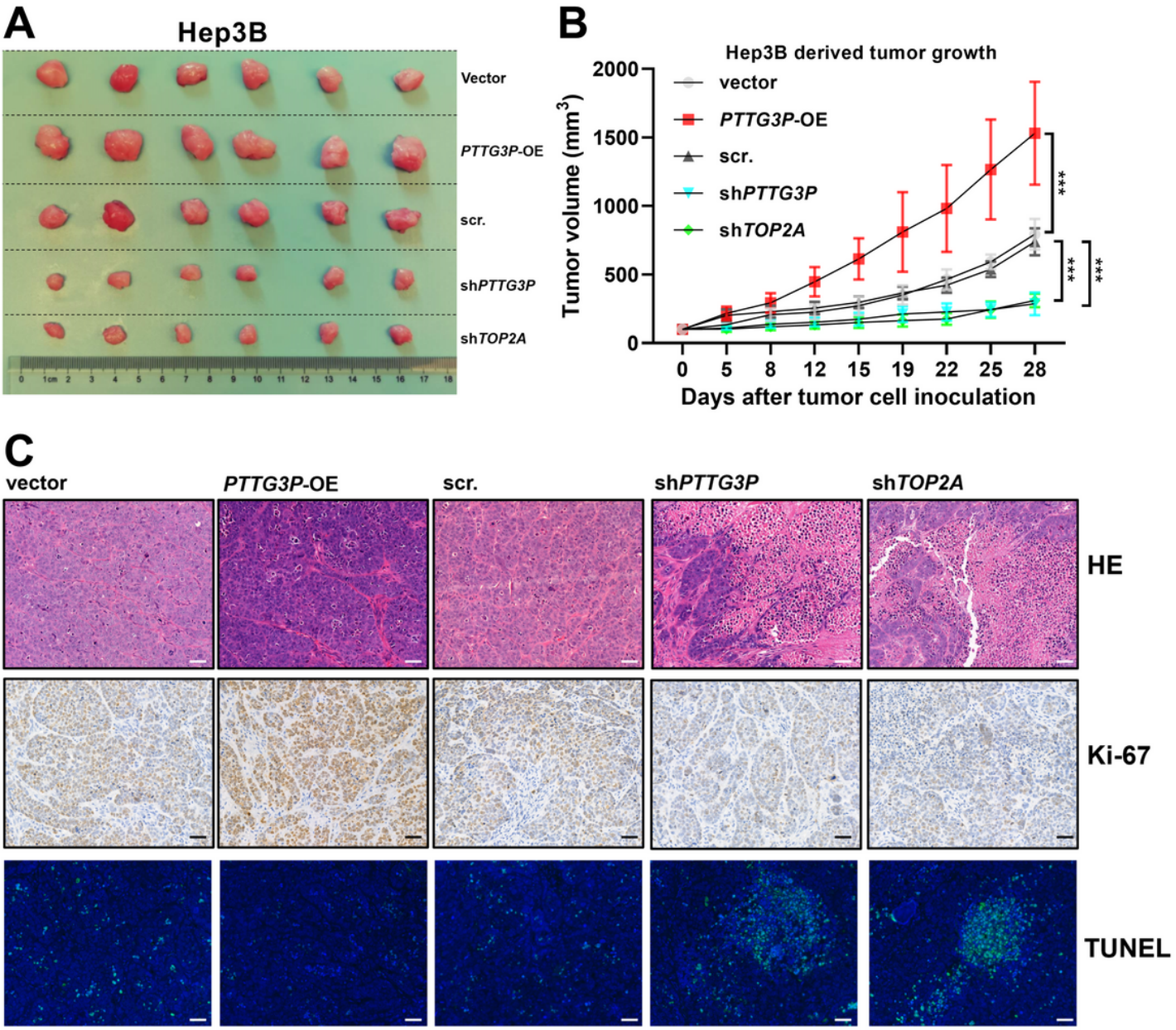

Figure 7

PTTG3P or *TOP2A* inhibition impaired HCC growth *in-vivo*

A-B. 6*10^5 Hep3B cells with *PTTG3P* overexpression, *PTTG3P* knockdown, or *TOP2A* knockdown were subcutaneously injected into the left or the right flanks of mice. 4 weeks after inoculation, the mice were sacrificed. Tumors were then removed and pictured (A) and the tumor growth curves are shown on the bottom (B). *, $p<0.05$; **, $p<0.01$; ***, $p<0.001$. **C.** Hematoxylin and eosin (H&E)-staining (top), IHC staining of Ki-67 (middle) and immunofluorescent staining of TUNEL (bottom) of paraffin-embedded sections obtained from tumor xenografts form each group in panel B. Scale bar is 50 μm.

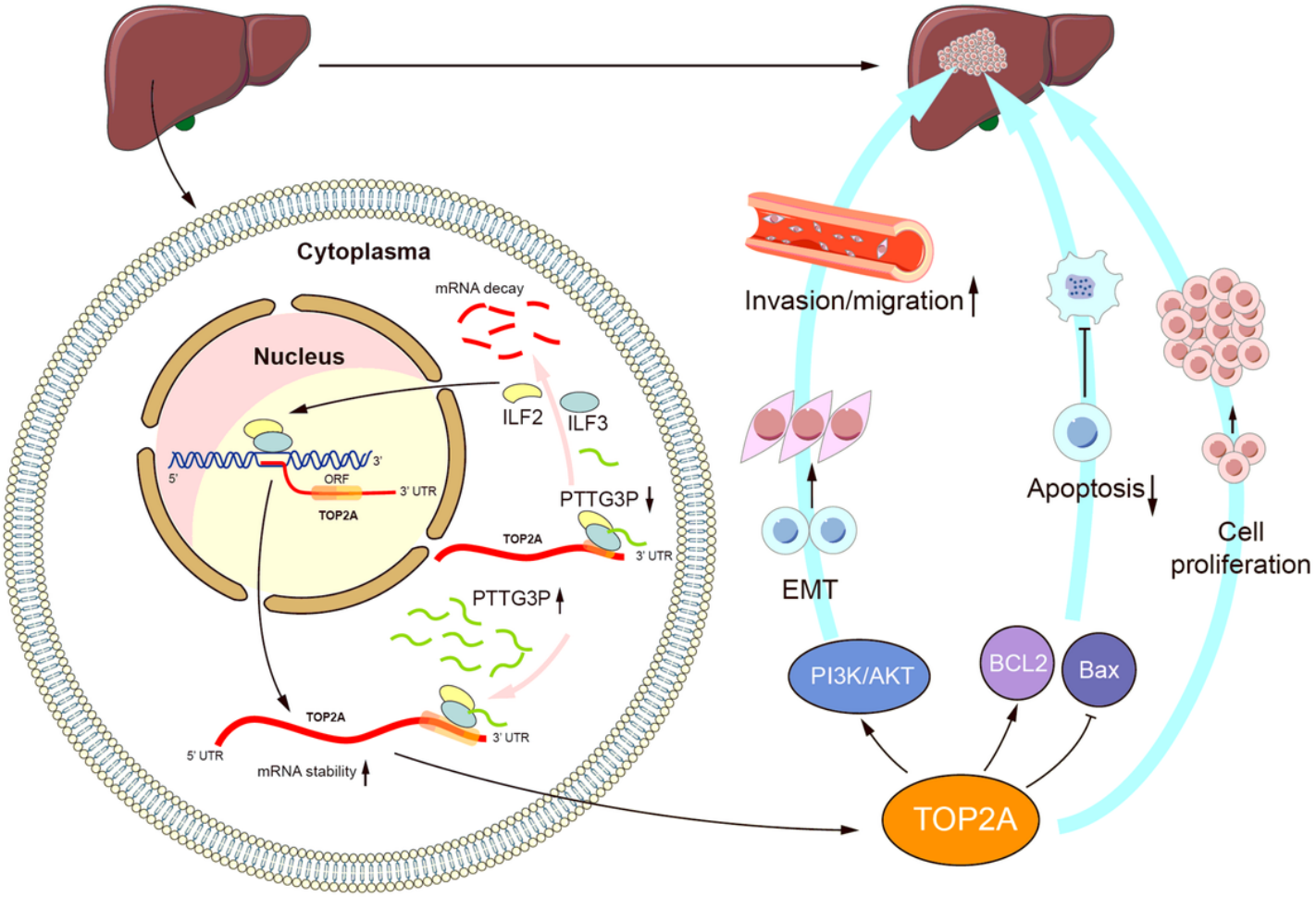

Figure 8

The regulatory mechanisms of PTTG3P on ILF2 distribution and function

A schematic image showing the regulatory mechanisms on ILF2 distribution, *TOP2A* transcription, and mRNA stability. *PTTG3P* forms a complex with ILF2/ILF3 in the cytoplasm of HCC cells. *PTTG3P* depletion promotes the nuclear translocation of ILF2, but not ILF3. The ILF2/ILF3 complex in the nuclear binds to the promoter of *TOP2A* and enhances its transcription.

Supplementary Files

This is a list of supplementary files associated with this preprint. Click to download.

- SupplementaryTable1PrimersandshRNA.xlsx
- SupplementaryTable2RNApulldownproteinlist.xlsx
- SupplementaryTable3.xlsx
- SupplementaryTable4.xlsx